


## Phase dependence of thermal transport in graphene Josephson junctions

Chuan-Shuai Huang \*

*Department of Physics, Xiamen University, Xiamen 361005, China*



(Received 12 February 2023; revised 9 September 2023; accepted 3 November 2023; published 27 November 2023)

We study theoretically the phase-dependent thermal transport in graphene-based Josephson junctions and highlight the role of Klein-like tunneling in the thermal energy transmission. We compute the thermal conductance for both short and long junctions by solving the Dirac-Bogoliubov–de Gennes equation. Numerical results show that the thermal conductance contains distinctive signatures of the existence of Andreev bound states, enabling us to identify different superconducting pairing symmetries in graphene, including  $s$ -,  $d_{x^2-y^2}$ -,  $d_{xy}$ -,  $p_x$ -, and  $p_y$ -wave symmetries. Importantly, our results may pave the way for applications of graphene in the field of Josephson heat interferometers.

DOI: [10.1103/PhysRevB.108.195433](https://doi.org/10.1103/PhysRevB.108.195433)

### I. INTRODUCTION

The phase-dependent heat currents in Josephson junctions were predicted more than half a century ago [1–3]. In such junctions, heat is carried by quasiparticles with energies above the superconducting gap. They can be transmitted across the junction in normal tunneling events as well as in Andreev-like processes where an electron-like quasiparticle is converted into a hole-like quasiparticle and vice versa together with the creation or annihilation of a Cooper pair in the condensate. It is these latter processes that give rise to the phase dependence of the thermal transport across a Josephson junction [4–7]. Over the past decade, a great deal of progress has been made in the Josephson heat interferometer, a temperature-biased superconducting quantum interference device, which allows full control of the coherent energy transfer through the Josephson junction [8–14]. These experimental breakthroughs led to the conception and implementation of various caloritronic devices, such as heat transistors [15,16], thermal diodes and switches [17–21], thermal memory [22], and refrigerators [23–25].

On the other hand, numerous theoretical works revealed that the detection of phase-dependent heat current is an effective method for studying the intrinsic physics of materials. For example, Josephson junctions' thermal signature can be utilized to investigate various phenomena such as the spin polarization of ferromagnets, topological superconductivity, localized Majorana end states, helical edge states of topological insulators, Andreev bound states (ABSs), and even unconventional pairing symmetry [26–32]. Recently, Savander *et al.* reported on the thermoelectric detection of ABSs in unconventional superconductors, since the Andreev thermoelectric effect is highly sensitive to surface states that emerge in unconventional superconductors [33]. However, to date, there have been no reports on the thermal transport of a graphene-based Josephson junction (GJJ).

Previous studies have demonstrated that graphene can exhibit various types of pairing symmetries through proximity effect, including  $s$ -wave,  $d$ -wave, and  $p$ -wave pairing [34,35]. The combination of these superconducting pairing symmetries with the relativistic low-energy Dirac fermions in graphene leads to a wide range of interesting physics and novel proximity effects [36,37]. Recent advancements in nanofabrication techniques, such as suspension of graphene or BN encapsulation, have further allowed for the realization of graphene Josephson junctions (GJJs) in the ballistic regime [36]. To apply GJJs to various caloritronic devices, e.g., graphene-based Josephson heat interferometers, it is an important issue to clarify the phase-dependent thermal transport properties of these junctions. Furthermore, the thermal conductance can provide clear evidence of the existence of ABSs, making it useful for distinguishing various pairing symmetries induced in graphene through thermal transport experiments.

In this paper, we mainly focus on the thermal transport in graphene-based superconductor–normal-metal–superconductor (SNS) junctions with different pairing symmetries and highlight the role of the relativistic Dirac fermions in the phase-dependent thermal conductance. Numerical results have revealed the phase dependence of the thermal conductance on various pairing symmetries, such as  $s$ -,  $d$ -, and  $p$ -wave symmetries. Importantly, we believe that understanding the phase-coherent heat transport in such junctions will be useful for the development of future superconducting quantum devices and nanotechnology. It might even reveal the potential applications of GJJs for smart energy control at mesoscopic scales and the management of heat dissipation at cryogenic temperatures.

### II. FORMALISM AND THEORY

We consider a two-dimensional graphene-based SNS junction in the  $x$ - $y$  plane, as depicted in Fig. 1, where the two interfaces are parallel to the  $y$  axis and located at  $x = 0$  and  $x = L$ , respectively. The N region of length  $L$  is a normal segment of graphene with a large electrostatic potential  $V_0$

\*245748852@qq.com

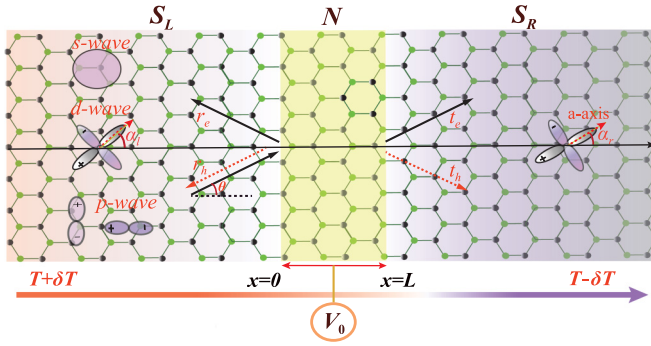


FIG. 1. (a) Schematic figure of graphene-based SNS junction constructed in the  $x$ - $y$  plane. Two superconducting electrodes  $S_L$  and  $S_R$ , separated by a distance  $L$ , are deposited in the left ( $l$ ,  $x < 0$ ) and right ( $r$ ,  $x > L$ ) regions, respectively. Thermal transport is driven by a temperature bias  $\delta T$  between the two superconducting electrodes. The sketch of the pairing configurations ( $s$  wave,  $p$  wave, and  $d$  wave) are denoted in the  $S_L$  and  $S_R$  regions.

induced by a tunable gate voltage. Here, we would like to emphasize that the junction along the  $y$  axis has a zigzag shape. According to the discussions in Refs. [38,39], the electron wave functions in such a junction with zigzag edges are assumed to be independent of valleys. The superconducting correlations between electron-hole excitations are described by Dirac-Bogoliubov-de Gennes (DBdG) equation [40],

$$\begin{bmatrix} H_{\pm} - E_F & \Delta(\mathbf{k}, \mathbf{r}) \\ \Delta^*(\mathbf{k}, \mathbf{r}) & E_F - H_{\pm} \end{bmatrix} \psi = E \psi, \quad (1)$$

where  $E$  is the excitation energy measured from the Fermi level  $E_F$ ,  $\psi = (u^e, v^e)^T$ , and  $(v^h, u^h)^T$  denote the wave functions of the electron- and hole-like excitations, respectively, and  $\Delta(\mathbf{k}, \mathbf{r})$  represents the proximity-induced superconducting pairing potential in graphene, which is  $\mathbf{k}$  dependent on the Fermi surface except for the isotropic  $s$ -wave pairing symmetry. In Eq. (1), the single-particle Hamiltonian is given by  $H_{\pm} = -i\hbar v_F (\sigma_x \partial_x \pm \sigma_y \partial_y) + V_0 \Theta(x) \Theta(-x + L)$  with the first term being the Dirac Hamiltonian, where  $v_F \simeq 10^6$  m/s is the Fermi velocity in graphene [41],  $\sigma_x$  and  $\sigma_y$  are Pauli matrices in the pseudospin space of the sublattices, and the indices  $\pm$  respectively stand for the  $K$  and  $K'$  valleys of graphene.  $V_0$  is an external gate voltage applied in the N region to create a tunneling barrier. Furthermore,  $\Theta$  is the Heaviside step function. Without losing generality, we neglect the smooth change of the pair potential in the vicinity of the SN interface, such that we may approximate their spatial dependence by a step function behavior  $\Delta(\mathbf{k}, \mathbf{r}) = \Delta_l(\mathbf{k}) e^{i\phi_l} \Theta(-x) + \Delta_r(\mathbf{k}) e^{i\phi_r} \Theta(x - L)$ . In our notation, the subscript  $i = l$  ( $r$ ) denotes the left (right) superconducting region. The temperature-dependent gap magnitude in the  $i$ th superconducting lead reads  $\Delta_i = \Delta_0 \tanh(1.74 \sqrt{T_c/T_i - 1})$  with  $\Delta_0 = 1.76 k_B T_c$  being the superconducting gap at zero temperature and  $T_c$  denoting the critical temperature [42]. Throughout this paper, the energies are normalized by  $\Delta_0$  and the temperature  $T_i$  is normalized by  $T_c$ . The mean-field approximation in superconducting regions is that  $E_F \gg \Delta_0$ , or equivalently, the Fermi wavelength in the superconducting region should be much smaller than the coherence length [43].

In light of this, we consider a heavily doped case with  $E_F = 100\Delta_0$ . Meanwhile, the Fermi momentum  $k_F$  in both  $S_L$  and  $S_R$  regions are assumed to be equal for simplicity.

The eigenfunctions of the DBdG equation describing electron-like quasiparticles (ELQs) and hole-like quasiparticles (HLQs) in the two superconductors are respectively given by

$$\begin{aligned} \psi_i^{e\pm}(x) &= (u_i^e, u_i^e e^{i\theta_{\pm}}, v_i^e e^{-i\phi_i^{\pm}}, v_i^e e^{i\theta_{\pm} - i\phi_i^{\pm}})^T e^{ik_i^e \cos \theta_{\pm} x}, \\ \psi_i^{h\pm}(x) &= (v_i^h, v_i^h e^{i\theta_{\pm}}, u_i^h e^{-i\phi_i^{\pm}}, u_i^h e^{i\theta_{\pm} - i\phi_i^{\pm}})^T e^{ik_i^h \cos \theta_{\pm} x}, \end{aligned} \quad (2)$$

where the coherence factors are written as  $u_i^{e(h)} = [(E + \Omega_i^{\pm})/2E]^{1/2}$  and  $v_i^{e(h)} = [(E - \Omega_i^{\pm})/2E]^{1/2}$  with  $\Omega_i^{\pm} = [E^2 - |\Delta_i^{\pm}(\theta)|^2]^{1/2}$  and the superscript  $e$  ( $h$ ) denoting the ELQ (HLQ). In Eq. (2), we have defined  $\theta_+ = \theta$  and  $\theta_- = \pi - \theta$  with  $\theta = \arctan(k_y/k_x)$  being the incident angle for an ELQ in the  $S_L$  region. To be more specific, the angle  $\theta$  describes the quasiparticle trajectory, the direction of the incident momentum relative to the interface normal. We have employed the weak-coupling limit, where the momentum  $\mathbf{k}$  is fixed on the Fermi surface, allowing us to effectively describe the  $\mathbf{k}$ -dependent pair potential as a function of angle  $\theta$ . In other words, we can express  $\Delta_i^{\pm}(\theta) = \Delta_i e^{i\phi_i^{\pm}} f(\theta_{\pm})$ , where  $f(\theta_{\pm})$  varies for different pairing symmetries. We have also defined  $e^{i\phi_i^{\pm}} = e^{i\phi_i} \Delta_i^{\pm}(\theta) / |\Delta_i^{\pm}(\theta)|$  with  $\phi_{i=l}$  ( $r$ ) being the macroscopic phase of superconductor  $S_L$  ( $S_R$ ). Note that there exists a phase difference  $\phi = \phi_l - \phi_r$  between the left and right superconductors. Furthermore, the related wave vectors are described as  $k_i^{e(h)} = [E_F + (-)\Omega_i^{\pm}]/\hbar v_F$ . Since the system has translational invariance in directions parallel to the interface, the transverse momenta  $k_y = k_i^{e(h)} \sin \theta_{\pm}$  are conserved in the scattering process.

The eigenfunctions for the N region are given by

$$\begin{aligned} \psi_n^{e\pm}(x) &= (1, \pm e^{\pm i\gamma_e}, 0, 0)^T e^{\pm ik_n^e x}, \\ \psi_n^{h\pm}(x) &= (0, 0, 1, \mp e^{\pm i\gamma_h})^T e^{\pm ik_n^h x}, \end{aligned} \quad (3)$$

with  $\gamma_e = \arcsin[\hbar v_F k_y / (E + E_F - V_0)]$ ,  $\gamma_h = \arcsin[\hbar v_F k_y / (E - E_F + V_0)]$ , the  $x$  component of the wave vectors  $k_n^e = (\hbar v_F)^{-1} (E + E_F - V_0) \cos \gamma_e$  and  $k_n^h = (\hbar v_F)^{-1} (E - E_F + V_0) \cos \gamma_h$ .

Let us now consider the situation where an ELQ  $\psi_l^{e+}$  is incident from the left-hand side ( $x < 0$ ). It gives rise to a backscattered ELQ  $\psi_l^{e-}$  or to an Andreev-reflected HLQ  $\psi_l^{h+}$ . Importantly, the incident quasiparticle can be also transmitted to the right-hand side ( $x > L$ ) as an ELQ  $\psi_r^{e+}$  or as an HLQ  $\psi_r^{h-}$ . Therefore, the wave functions in the  $S_L$  and  $S_R$  regions can be expressed as  $\Psi_L = \psi_l^{e+} + r_e \psi_l^{e-} + r_h \psi_l^{h+}$  and  $\Psi_R = t_e \psi_r^{e+} + t_h \psi_r^{h-}$ , respectively. In addition, the wave function in the N region  $\Psi_N$  can be constructed using Eq. (3). We remark that the electron-like and hole-like states in the  $S_L$  and  $S_R$  regions are different due to the temperature bias across the junction. The transmitted amplitudes  $t_e$  and  $t_h$  can be determined by matching the boundary conditions at  $x = 0$  and  $x = L$ :

$$\Psi_L|_{x=0-} = \Psi_N|_{x=0+}, \quad \Psi_N|_{x=L-} = \Psi_R|_{x=L+}. \quad (4)$$

The thermal energy is carried by the quasiparticles with energy  $E > \Delta(\theta)$  and the transmission probability can be

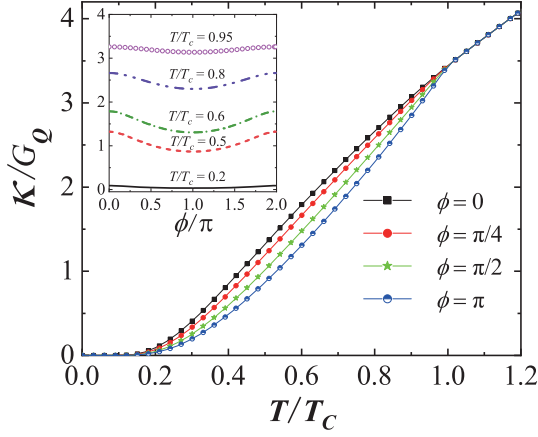


FIG. 2. (a) Thermal conductance as a function of  $T/T_c$  for various phase difference  $\phi$  in the transparent limit. Inset shows the phase-dependent thermal conductance  $\kappa(\phi)$  for different values of  $T/T_c$ . Thermal conductance is normalized by the heat flux quantum  $G_Q = 4\pi^2 k_B^2 T / (3h)$ .

expressed as  $\tilde{\tau}(E, \theta) = |t_e|^2 + |t_h|^2$ . Similarly, for an incident HLQ, we can also obtain the transmission probability  $\tilde{\tau}'(E, \theta) = |t'_e|^2 + |t'_h|^2$ . By assuming a temperature bias  $\delta T$  across the SNS junction, the thermal conductance averaging over all possible incident angles  $\theta$  is given by [27,31,44]

$$\kappa(\phi) = \frac{4}{h} \int_{-\pi/2}^{\pi/2} d\theta \cos \theta \int_{\Delta(\theta)}^{\infty} dE E [\tilde{\tau}(E, \theta) + \tilde{\tau}'(E, \theta)] \frac{df}{dT}. \quad (5)$$

Therein,  $f = (e^{E/k_B T} + 1)^{-1}$  denotes the equilibrium Fermi distribution. We emphasize that this formula is valid for both isotropic and anisotropic pairing symmetries. The thermal conductance is normalized by  $G_Q = 4\pi^2 k_B^2 T / (3h)$  with  $\pi^2 k_B^2 T / (3h)$  being the thermal conductance quantum [45]. The degeneracy factor four accounts for the spin and valley degeneracies of graphene.

### III. RESULTS AND DISCUSSION

#### A. Graphene-based SNS junction with $s$ -wave pairing

For  $s$ -wave pairing, we have  $\Delta(\theta) \equiv \Delta$ , meaning that the energy gap is isotropic and independent of the momentum. We first focus on the thermal transport in a short junction limit, where the junction length  $L$  is much smaller than the superconducting coherence length  $\xi_0 = \hbar v_F / \Delta_0$ . In this case, it is possible to model the N region by a  $\delta$ -shaped barrier located at the interface between the two superconductors, characterized by a dimensionless parameter  $Z = V_0 L / \hbar v_F$ , which represents the barrier strength [46–48]. In this approach, we take the limit  $d \rightarrow 0$  and  $V_0 \rightarrow \infty$ , such that  $\gamma_e \rightarrow 0$ ,  $\gamma_h \rightarrow 0$ ,  $-k_n^e L = (-E - E_F + V_0)L / \hbar v_F \rightarrow Z$ , and  $k_n^h L = (E - E_F + V_0)L / \hbar v_F \rightarrow Z$ .

Consider first the situation of a transparent junction, corresponding to  $Z = 0$ . Figure 2(a) shows the normalized thermal conductance  $\kappa/G_Q$  versus the temperature  $T$  for various phase differences  $\phi = \phi_l - \phi_r$ . It has been observed that when the temperature is below the transition temperature  $T_c$ ,  $\kappa/G_Q$  exhibits an exponential increase with respect to  $T/T_c$ . This

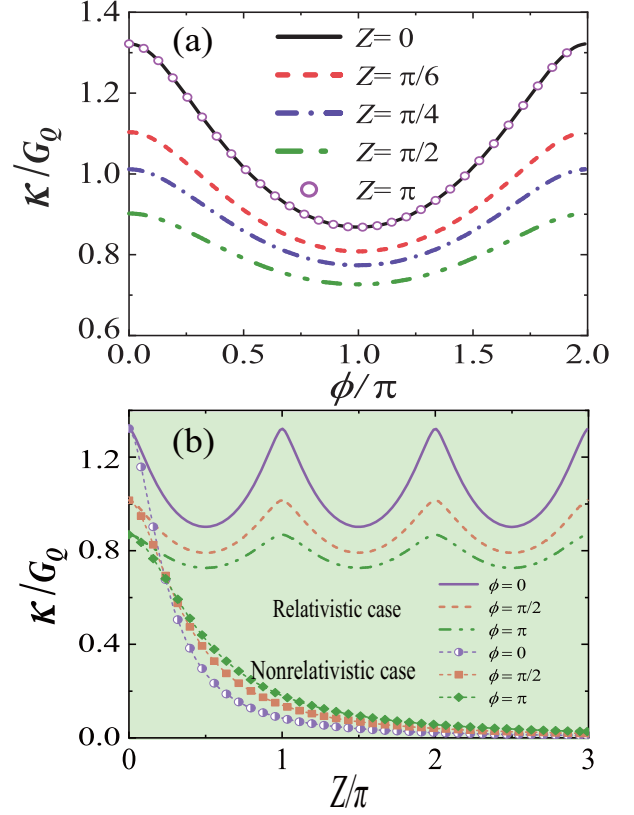


FIG. 3. (a) The phase-dependent thermal conductance  $\kappa(\phi)$  for various barrier strengths  $Z$  at  $T/T_c = 0.5$ . (b) Comparison of  $\kappa(Z)$  between the relativistic and nonrelativistic cases at  $\phi = 0, \pi/2$  and  $\pi$ .

behavior is indicative of the spherical symmetry associated with  $s$ -wave pairing. For  $T > T_c$ , the  $S_L$  ( $S_R$ ) part fades into a normal state, causing the heat transport to exhibit a linear dependence on temperature regardless of the change in  $\phi$ , which coincides with the Wiedemann-Franz law for normal metals in low temperatures [45,49]. In other words, the thermal conductance at  $T > T_c$  is proportional to temperature, i.e.,  $\kappa \propto T$ . The phase dependence of the thermal conductance for different values of  $T$  is shown in the inset of Fig. 2. One can see that  $\kappa(\phi)$  is  $2\pi$  periodic and has a minimum at  $\phi = \pi$ , and varying temperature cannot change the qualitative features of  $\kappa(\phi)$  except for the magnitude of the oscillation with respect to  $\phi$ . Raising the temperature from  $0.2T_c$  to  $0.6T_c$  could enhance the oscillating amplitude of  $\kappa(\phi)$  due to the increase of thermal energy transmission carried by quasiparticles above the superconducting gap. However, as the temperature approaches  $T_c$ , the oscillating amplitude tends to zero. This is because higher temperatures decrease the magnitude of the gap  $\Delta$ , thereby diminishing the effects of quantum phase coherence. Therefore, from an experimental perspective, the optimal conditions for detecting the phase dependence occur at intermediate temperatures, such as  $T = 0.5T_c$  and  $0.6T_c$ . Next, we investigate the effect of the tunneling barrier on  $\kappa(\phi)$ , as depicted in Fig. 3(a), where we consider a series of barrier strengths ranging from  $Z = 0$  to  $Z = \pi$ . The thermal conductance is found to decrease as expected when the junction transparency

is reduced. Notably,  $\kappa(\phi)$  consistently displays a minimum at  $\phi = \pi$  regardless of the barrier height. This phenomenon is in contrast with the nonrelativistic case, which has been studied in Refs. [27,31,32]. In the nonrelativistic case, a minimum at  $\phi = \pi$  is observed only at high transparency, whereas in the tunneling limit, the thermal conductance becomes maximal at  $\phi = \pi$ . Such a distinction becomes even clearer when plotting the thermal conductance as a function of  $Z$  for three values of phase differences:  $\phi = 0$ ,  $\phi = \pi/2$ , and  $\phi = \pi$ , as shown in Fig. 3(b). For comparison, the corresponding  $\kappa(\phi)$  for the nonrelativistic case is also calculated and indicated by the line-symbol curves, which reproduces the qualitative findings of Refs. [31,32]. It is observed in Fig. 3(b) that, for the relativistic case,  $\kappa(Z)$  at  $\phi = 0$  is always larger than that at  $\phi = \pi$ . More importantly,  $\kappa(Z)$  appears as a periodic function with a period of  $\pi$ , indicating the thermal energy's Klein-like tunneling. Such a periodic behavior is a direct manifestation of the relativistic low-energy Dirac fermions [46–48], which cannot be observed in conventional SNS junctions. One can see that the thermal conductance in the nonrelativistic case always shows an exponential dependence on the tunneling barrier  $Z$ . Note also that the three line-symbol curves intersect at  $Z \approx \pi/4$ , implying that  $\kappa(\phi)$  at  $\phi = \pi$  will undergo a transition from minimal to maximal thermal conductance as  $Z$  increases.

Those distinct features of  $\kappa(\phi)$  can be understood by analyzing the transmission function  $\tau(E, \phi)$  as well as the ABSs localized in the N region, as shown in Fig. 4. Since the thermal conductance receives contributions from quasiparticles approaching the junction at all angles of incidence, the transmission function  $\tau(E, \phi)$  is defined as an integral over  $\theta$ , i.e.,  $\tau(E, \phi) = \int_{-\pi/2}^{\pi/2} d\theta \cos \theta [\tilde{\tau}(E, \theta) + \tilde{\tau}'(E, \theta)]$ . We would like to emphasize that the phase-dependent thermal transport arises due to thermally excited quasiparticles above the superconducting gap, as pointed out in Refs. [26–32]. In other words, it depends explicitly only on the quasiparticle spectrum above the gap. The subgap ABSs do not contribute to stationary thermal transport, as these particles can only enter the superconducting banks by condensing into a Cooper pair, which carries no heat. More specifically, electrical transport is possible via ABSs for energies within the excitation gap  $\Delta(\theta)$ , i.e.,  $E < \Delta(\theta)$ . Conversely, thermal transport is completely hindered, as evanescent waves with excitation energy  $E < \Delta(\theta)$  cannot be transmitted through the SNS junction. Then, as seen in the Eq. (5), the thermal conductance is integrated from  $E = \Delta(\theta)$  to  $E \rightarrow \infty$ . The sensitivity of  $\kappa(\phi)$  to ABSs within the pairing gap is a result of the direct connection between thermal conductance and the superconductor's density-of-states. The detailed solution for ABSs can be found in the Appendix.

For the nonrelativistic case, the  $\theta$ -dependent ABS can be expressed as  $E_b(\theta, \phi) = \pm \Delta [\cos^2(\phi/2) + (1 - \tilde{\sigma}_n) \sin^2(\phi/2)]^{1/2}$  with  $\tilde{\sigma}_n$  being the transmission probability of the junction in the normal state [50]. By introducing the  $\delta$ -function barrier model, we have  $\tilde{\sigma}_n = \cos^2 \theta / (\cos^2 \theta + Z^2)$ . Note that the interface transparency can be characterized by the value of  $\tilde{\sigma}_n$ . In the transparent limit, i.e.,  $\tilde{\sigma}_n \approx 1$ , the ABS at  $\phi = \pi$  goes to zero energy. This low-energy ABS removes the density of states from above the superconducting gap  $\Delta$ , causing a

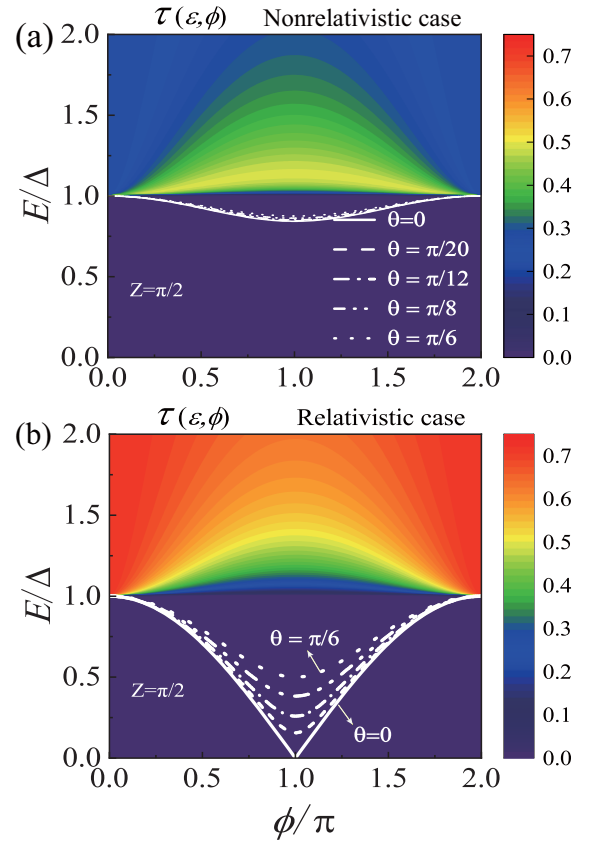


FIG. 4. Transmission function  $\tau(E, \phi)$  of a SNS Josephson junction with  $s$ -wave pairing in (a) the nonrelativistic case and (b) the relativistic case. White lines inside the superconducting gap indicate the energy of ABSs for various incident angles ( $\theta$ , from 0 to  $\pi/6$ ). The temperature is set to  $T/T_c = 0.5$  and the barrier strength is set to  $Z = \pi/2$ . The thermal conductance receives contributions from quasiparticles approaching the junction at all angles of incidence, such that  $\tau(E, \phi)$  is an integral of  $\theta$ .

reduction in thermal energy transmission at  $\phi = \pi$ , which is not shown here. As can be seen from Fig. 4(a) for  $Z = \pi/2$ , corresponding to a junction with low transparency where  $\tilde{\sigma}_n$  is strongly suppressed, the ABS energy at  $\phi = \pi$  moves up to the gap edge, giving rise to a resonant transmission for quasiparticles with energies slightly above  $\Delta$ . This in turn enhances the thermal conductance at  $\phi = \pi$ , leading to a phase shift of  $\kappa(\phi)$  as  $Z$  increases.

However, this is not the case for graphene with relativistic DBdG quasiparticles. The  $\theta$ -dependent ABS for GJJs with  $s$ -wave pairing can be obtained as [51]

$$E_b(\theta, \phi) = \pm \Delta \sqrt{1 - \sigma_n \sin^2(\phi/2)},$$

$$\sigma_n = \frac{\cos^2 \theta}{1 - \cos^2 Z \sin^2 \theta}. \quad (6)$$

Therein,  $\sigma_n$  is the angularly resolved transmission coefficient of this graphene junction in the normal state. Owing to the Klein tunneling, quasiparticles in the normal state with normal incidence always exhibit unit transmission [i.e.,  $\sigma_n(\theta = 0) \equiv 1$ ] regardless of the height of the barrier potential.

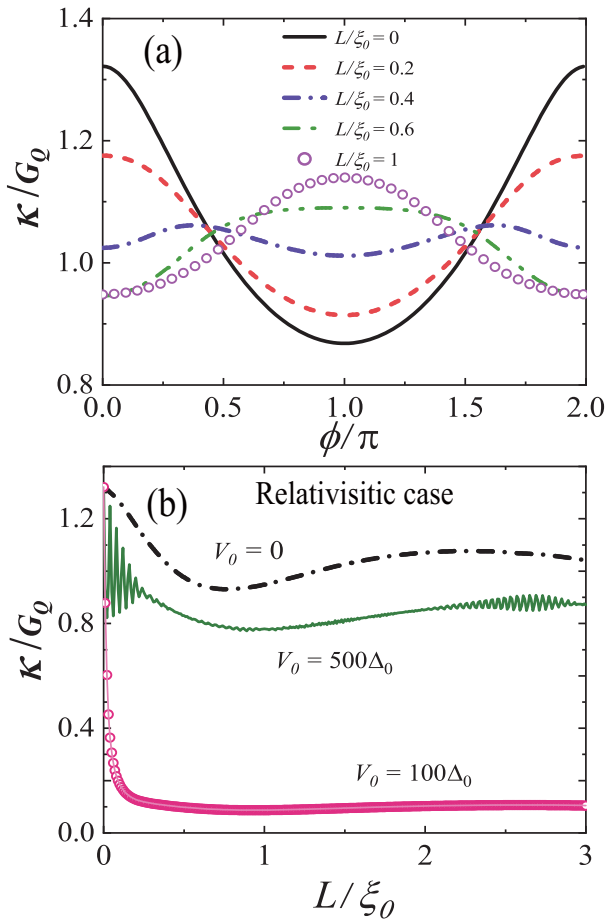


FIG. 5. (a) The phase-dependent thermal conductance  $\kappa(\phi)$  for various junction lengths  $L/\xi_0$  at  $V_0 = 0$ . (b) Thermal conductance as a function of  $L/\xi_0$ , and the related parameters are denoted in the figure. The temperature is fixed at  $T/T_c = 0.5$ .

Consequently, the ABS energies for small incident angles (e.g.,  $\theta < \pi/6$ ) stay close to the zero energy at  $\phi = \pi$ , as seen in Fig. 4(b). These low-energy ABSs diminish the magnitude of the corresponding thermal conductance as discussed previously. Since the heat current is predominantly contributed by quasiparticles at small incident angles, a junction like this can always display a minimal thermal conductance at  $\phi = \pi$ , even when the barrier potential is very large. We would like to point out that this behavior is not exclusively unique to topological ABSs and Majorana fermions mentioned in Refs. [27,31,32]. Rather, it originates from the Klein-like tunneling of relativistic DBdG quasiparticles.

So far, the above discussions are restricted to the short-junction limit. Now, we extend our analysis to the case of a long junction made of graphene. It is important to consider the junction length in relation to the superconducting coherence length, which can be quantified as  $\xi_0 = \Delta_0/\hbar v_F$ . In Fig. 5(a), we present the phase-dependent thermal conductance for different junction lengths normalized by  $\xi_0$ , denoted as  $L/\xi_0$ . It is evident that the phase dependence is significantly affected by varying  $L/\xi_0$ . The minimum of  $\kappa(\phi)$  is no longer situated at  $\phi = \pi$ , but instead gradually shifts to  $\phi = 0$  as  $L$  increases, and we can define this phenomenon as a  $\phi$  junction. Such a phase shift in  $\kappa(\phi)$  is reminiscent of the skewness observed

in the supercurrent curve  $I(\phi)$  [52–55]. Both phenomena are linked to the high transmission of quasiparticles due to the Klein-like tunneling effect. However, the underlying physical mechanisms driving these two phenomena are different. The former is attributed to the momentum difference between electrons and holes, i.e.,  $k_n^e - k_n^h = 2E/\hbar v_F$ , which is a direct consequence of the Dirac-like energy dispersion for graphene. The latter, on the other hand, arises from the exceptionally high transparency of the interface between graphene and a superconductor.

Figure 5(b) illustrates the dependence of thermal conductance on  $L$  for different values of  $V_0$  at  $\phi = 0$ . For  $V_0 = 0$ , the thermal conductance exhibits an oscillatory pattern as a function of  $L$ , where the amplitude of these oscillations is damped over a distance comparable to the superconducting coherence length  $\xi_0$ . Our findings reproduce the qualitative observations described in Ref. [27]. The situation changes dramatically when we consider the case of  $E_F = V_0 = 100\Delta_0$ , where the Fermi level of the N region is located at Dirac points, corresponding to undoped graphene. Since the density of states vanishes at the Dirac point, the transmission through a strip of undoped graphene occurs entirely via evanescent (exponentially decaying) modes. For a short and wide strip ( $W/L \gg 1$ ), there is a large number of evanescent modes with transmission probabilities of order unity. The transmission probabilities of these evanescent modes are the same as those of diffusive modes in a disordered piece of metal with the same conductance. As pointed out in Ref. [38], this peculiar transport characteristic can be understood as “pseudodiffusive dynamics.” As illustrated in Fig. 5(b), the thermal conductance exhibits an exponential decay as  $L$  increases, indicating pseudodiffusive dynamics, where the transport is not purely diffusive but rather a combination of diffusive and ballistic behavior. Understanding and controlling these dynamics is crucial for the development of graphene-based electronic devices.

If  $V_0$  is further increased up to  $500\Delta_0$ , the N region can be deemed as a square potential barrier. Many distinguishing features can be extracted from inspecting Fig. 5(b) for  $V_0 = 500\Delta_0$ . As seen, the thermal conductance  $\kappa$  versus  $L$  exhibits a series of resonance peaks. The condition for these resonant tunneling processes can be approximately expressed as  $kL \sim (E_F - V_0)L/\hbar v_F = n\pi$ . Such a resonance phenomenon is strongly dependent on the height of the potential barrier, which can provide a distinct experimental signature of the thermal energy’s Klein-like tunneling. One immediate advantage of this graphene-based hybrid system is the highly efficient heat dissipation even when the interface is not perfect so as to produce a large barrier, thus overcoming the limitation imposed by the large barrier induced in a conventional SNS junction due to the imperfect interface.

We again emphasize that those findings discussed above can serve as characteristic features of DBdG quasiparticles rather than being unique to topological ABS and Majorana fermions discussed in Ref. [27].

## B. Graphene-based SNS junction with $d$ -wave pairing

It has been widely accepted that such high- $T_c$  superconductors as  $\text{YBa}_2\text{Cu}_3\text{O}_{7-\delta}$  (YBCO) have a  $d$ -wave pairing

symmetry. In doped graphene,  $d$ -wave symmetry has recently been suggested to emerge from electron-electron interactions, which is intimately linked to the hexagonal crystal lattice [56]. Recently, the fabrication of graphene/YBCO contacts and their superconducting proximity effect have been reported [57–60]. The so-called Klein-like tunneling of Andreev electron-hole pairs that carry superconducting correlations from YBCO into graphene has also been experimentally observed [59]. Moreover, the role of  $d$ -wave pairing symmetry in the Josephson current based on graphene has been also studied, demonstrating that the current is significantly affected by the anisotropic pairing [61,62]. Understanding and controlling the emergence of  $d$ -wave symmetry in graphene has the potential to unlock new possibilities for the design of novel electronic devices. In what follows, we are going to discuss the phase-dependent thermal transport in GJJs with  $d$ -wave pairing.

To account for the effect of the  $d$ -wave pairing, we choose the  $d_{x^2-y^2}$  gap which in the weak-coupling approximation reads  $\Delta_i^\pm(\theta) = \Delta \cos(2\theta \mp 2\alpha_i)$  with  $i = l, r$ . Here,  $\alpha_i$  is the angle formed by the crystallographic  $a$  axis of the  $\text{CuO}_2$  plane and the interface normal (i.e.,  $x$  axis) as illustrated in Fig. 1. It can be also understood as the relative orientation of the gap in  $\mathbf{k}$  space with respect to the interface normal. If one rotates a  $d$ -wave superconductor on one side of the junction by an angle of  $\pi/2$ , e.g.,  $\alpha_l \rightarrow \alpha_l + \pi/2$ , the junction's characteristic is interchanged due to the sign change of the superconducting order parameter on the Fermi surface. Physically, it is interesting to consider the case of  $\alpha = \alpha_l = -\alpha_r$  [63,64]. By doing so, the orientations of the order parameters on the left and right sides are mirror-symmetric with respect to the interface normal, such that it is possible to form zero-energy bound states (ZESs) at the junction interface by rotating  $\alpha$  [63–66].

Turning now to the role of  $d$ -wave pairing in thermal transport, we first consider a short junction in the transparent limit. In Fig. 6(a), we show the thermal conductance versus the temperature  $T$  for various crystal misorientation angles within the range  $\alpha \in [0, \pi/4]$ . The phase difference between  $S_L$  and  $S_R$  regions is fixed at  $\phi = \pi$ . For comparison, the corresponding  $\kappa(T)$  for  $s$ -wave pairing is also plotted and indicated by the black-solid curve. For  $T < T_c$ , the thermal conductance for  $\alpha = 0$  shows an exponential increase versus  $T$  similar to that of the  $s$ -wave case. However, when  $\alpha$  is rotated to  $\pi/8$ , both the magnitude and the slope of  $\kappa(T)$  exhibit a remarkable enhancement. With further increasing  $\alpha$ , the Wiedemann-Franz law can be observed even at temperatures below  $T_c$ , providing an important experimental signature of gap nodes in  $d$ -wave superconductors. More specifically, as  $\alpha$  rotates from 0 to  $\pi/4$ , the nodal direction of  $d$ -wave pairing gradually shifts towards the interface normal, allowing more quasiparticles to tunnel into the gap nodes. This leads to a significant enhancement of the thermal conductance and reduces the impact of  $\Delta$  on quasiparticle tunneling below the critical temperature. Additionally, it is worth noting from the inset of Fig. 6(a) that  $\kappa$  exhibits a periodic dependence on  $\alpha$  with a period of  $\pi/2$ , highlighting the importance of the angle  $\alpha$  in modulating the thermal conductance.

The phase dependence of the thermal conductance for different  $\alpha$  is illustrated in Fig. 6(b). The most striking aspect here is the phase shift of  $\kappa(\phi)$  induced by rotating  $\alpha$ .

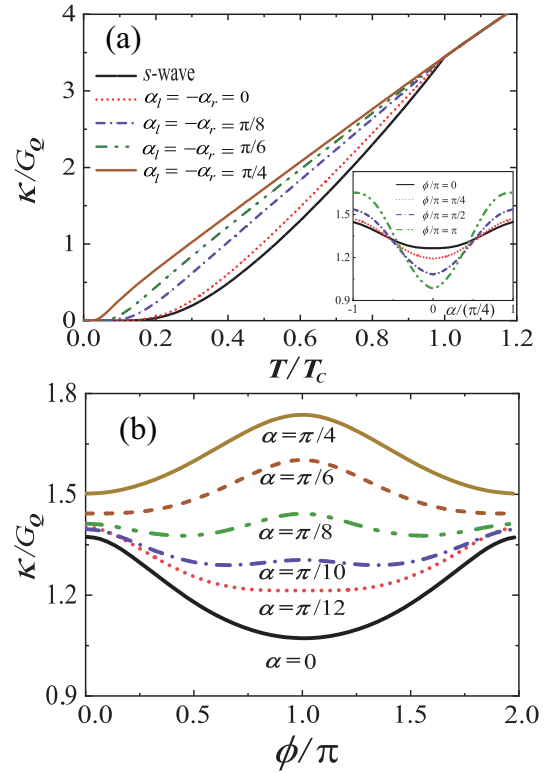


FIG. 6. (a) Thermal conductance as a function of  $T/T_c$  for various misorientation angles of  $d$ -wave pairing ( $\alpha = 0 - \pi/4$ ) in the transparent limit, where the phase difference is chosen as  $\phi = \pi$ . Inset shows the  $\alpha$ -dependent thermal conductance for different  $\phi$ . (b) Phase-dependent thermal conductance  $\kappa(\phi)$  for a series values of  $\alpha$  at  $T/T_c = 0.5$ .

Specifically, at  $\phi = \pi$ , the thermal conductance undergoes a transition from a minimum value to a peak value as  $\alpha$  increases from 0 to  $\pi/4$ . This explicitly demonstrates that the nodal direction of the superconducting order parameter plays a vital role in determining the phase dependence of thermal transport. Next, we proceed to calculate the effect of barrier potential on  $\kappa(\phi)$ . The temperature is set at  $T = 0.5T_c$ . For  $\alpha = 0$ ,  $\kappa(\phi)$  always exhibits a minimum at  $\phi = \pi$ , regardless of the increase in  $Z$ , as shown in Fig. 7(a). This behavior is similar to that shown in Fig. 3(a) for the  $s$ -wave case. For  $\alpha_l = -\alpha_r = \pi/4$ , as shown in Fig. 7(b), there is always a thermal conductance peak at  $\phi = \pi$ . This can be also observed clearly in the periodic oscillatory behavior of  $\kappa(Z)$  shown in Figs. 7(c) and 7(d). Therefore, we conclude that for GJJs with  $d$ -wave pairing, the tunneling barrier cannot qualitatively change the phase dependence of thermal conductances.

To gain a deep insight into the contrast behavior of  $\kappa(\phi)$  for  $\alpha = 0$  and  $\alpha = \pi/4$ , it is instructive to consider analytically the expression of ABSs for the GJJ with  $d$ -wave pairing. For  $\alpha = 0$ , the ABS is given by [62]

$$E_b(\theta, \phi) = \pm |\Delta \cos(2\theta)| \sqrt{1 - \sigma_n \sin^2(\phi/2)}. \quad (7)$$

This expression is formally equivalent to the ABS for GJJs with  $s$ -wave pairing, except that the gap now displays angular dependence, i.e.,  $\Delta(\theta) = \pm \Delta \cos(2\theta)$ . Therefore, one would expect qualitatively the same results for the thermal

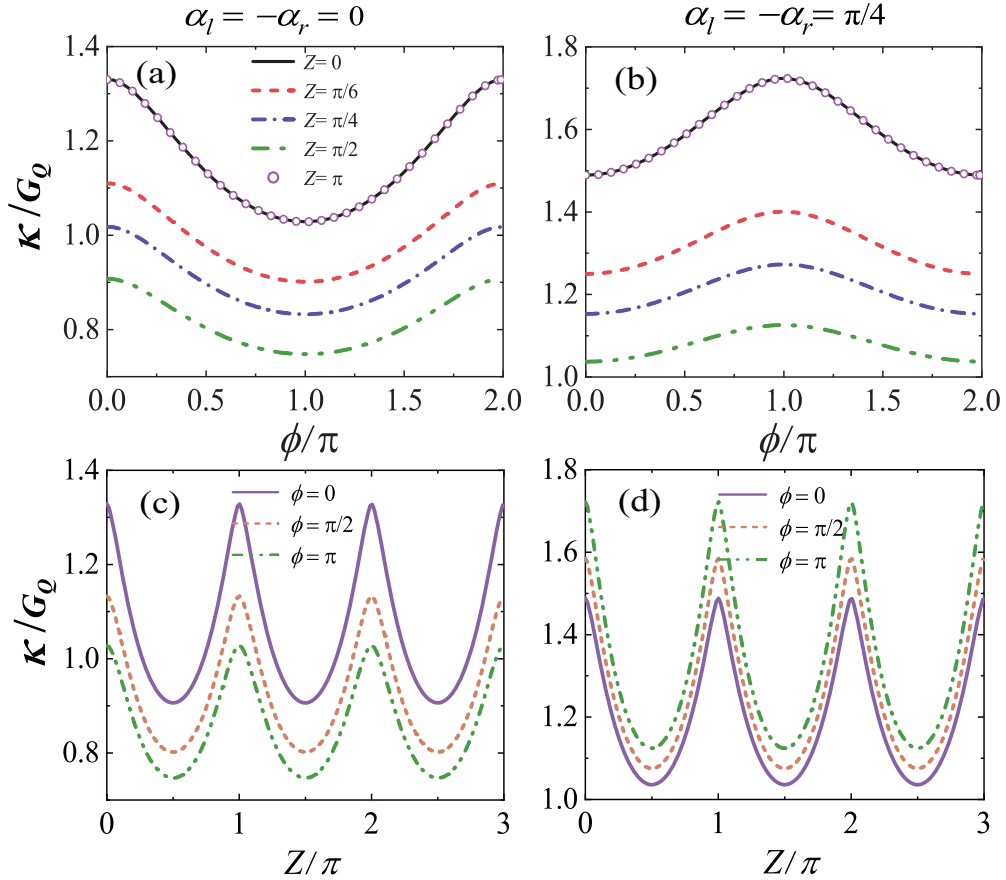


FIG. 7. Phase-dependent thermal conductance  $\kappa(\phi)$  for a series values of  $Z$  at (a)  $\alpha = 0$  and (b)  $\alpha = \pi/4$ . Comparison of  $\kappa(Z)$  between the cases of (c)  $\alpha = 0$  and (d)  $\alpha = \pi/4$ . The temperature is fixed at  $T/T_c = 0.5$ .

conductance when comparing the  $d$ -wave case with the  $s$ -wave case. The  $\phi$  dependence of  $E_b$  for different  $\theta$ , as well as the transmission function  $\tau(\phi, E)$ , is plotted in Fig. 8(a), where the barrier strength is fixed at  $Z = \pi/2$ . Due to the existence of energy-gap nodes in  $d$ -wave superconductors, there are unpaired single-particles tunneling into the gap, which is evident from the transmission function for energies within the energy gap ( $E < \Delta$ ). In other words, the quasiparticles have the ability to leak in and out of the Andreev bound states (ABSs). This leakage mechanism allows for the heat current to be carried by quasiparticles with energies below the superconducting gap. Note also that the transmission function for  $E < \Delta$  is nearly independent of  $\phi$ . However, the amplitude of these transmissions is much lower than that in the case of  $E > \Delta$ , meaning that the impact on  $\kappa(\phi)$  from these transmissions is not significant.

For  $\alpha_l = -\alpha_r = \pi/4$ , the ABS is given by [61]

$$E_b(\theta, \phi) = \pm |\Delta \sin(2\theta)| \sqrt{\sigma_n} \sin(\phi/2). \quad (8)$$

From this expression, it can be observed that there are always a pair of ZESs at  $\phi = 0, 2\pi$  regardless of the value of  $Z$ . These robust ZESs originate from the sign change of the pairing potential on the Fermi surface, namely,  $\Delta_i(\theta_+) = -\Delta_i(\theta_-)$ , which is a characteristic feature for superconductors with  $d_{xy}$ -wave pairing [65,66]. As seen in Fig. 8(b), the zero energies of ABSs at  $\phi = 0, 2\pi$  prevent the resonant tunneling, as discussed in the previous cases at  $\phi = \pi$ . This can be directly

responsible for the robust minimal thermal conductance at  $\phi = 0, 2\pi$ . Moreover, the peaks of ABSs appear exactly at  $\phi = \pi$ , resulting in resonance physics at  $\phi = \pi$ , which explains the thermal conductance peak at this phase. On the other hand, considering that the nodal direction in the  $\alpha = \pi/4$  configuration is aligned with the interface normal, there will more unpaired quasiparticles tunneling into the gap nodes when compared with the case of  $\alpha = 0$ . As a consequence, the thermal conductance for  $\alpha = \pi/4$  is significantly enhanced [see Fig. 6(b)].

In regards to the intermediate values of  $\alpha$ , i.e.,  $0 < |\alpha| < \pi/4$ , we have  $|\Delta_i(\theta_+)| \neq |\Delta_i(\theta_-)|$ . In this case, the actual sign change of the pairing potential or the condition for the formation of ZESs depends on the angle  $\theta$ . More specifically, the two pair potentials have opposite signs only within the range of  $\pm\pi/4 - |\alpha| < \theta < \pm\pi/4 + |\alpha|$ . In this range, robust ZESs can be formed at  $\phi = 0, 2\pi$ , while they are absent for the other incident modes. Nonetheless, when  $\alpha$  is rotated to approximately  $\pi/8$ , the ZESs become dominant among the incident modes, thereby causing a phase shift in  $\kappa(\phi)$ . This is why the phase dependence of thermal conductances is highly sensitive to  $\alpha$ .

We now turn to the case of a long SNS junction with  $d$ -wave pairing and compare the behavior of  $\kappa(\phi)$  for  $\alpha = 0$  and  $\alpha = \pi/4$ . The phase-dependent thermal conductance for a series of junction length  $L/\xi_0$  is plotted in Fig. 9. Similar to the  $s$ -wave case,  $\kappa(\phi)$  undergoes a phase shift with the

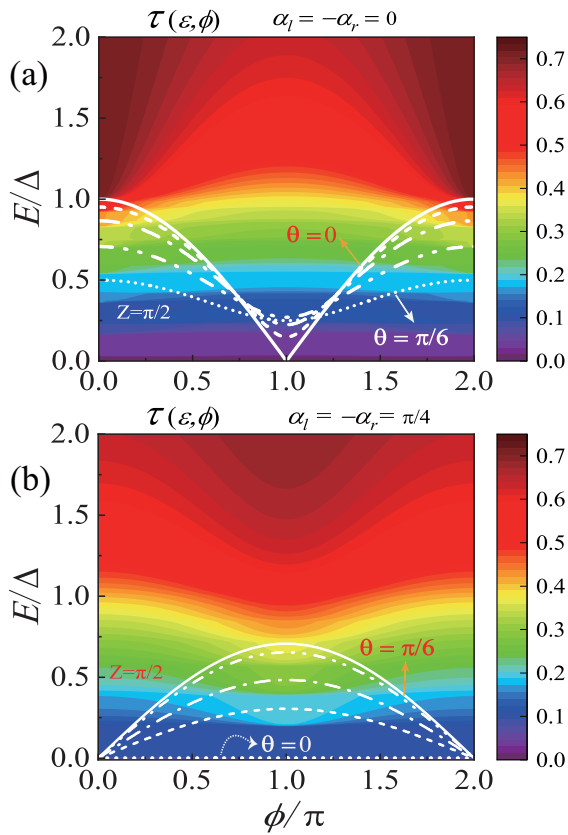


FIG. 8. Transmission function  $\tau(E, \phi)$  of a SNS junction with  $s$ -wave pairing at (a)  $\alpha = 0$  and (b)  $\alpha = \pi/4$ , corresponding to Figs. 7(a) and 7(b), respectively. White lines inside the superconducting gap indicate the energy of ABSs for various incident angles ( $\theta$ , from 0 to  $\pi/6$ ). The other parameters are the same as those in Fig. 4.

increase of  $L$  on the scale of  $\xi_0$ . Of particular importance is the observation that the ground states of  $\kappa(\phi)$  for  $\alpha = 0$  and  $\alpha = \pi/4$  are always opposite regardless of the ratio of  $L/\xi_0$ . The experimental observation of this unique feature may serve as a conclusive proof for the  $d$ -wave pairing and also the best judgment about the formation of zero-energy ABS.

Overall, we have found that the phase-coherent thermal transport in GJJs with  $d$ -wave pairing differs significantly from that in the  $s$ -wave case. The distinction is particularly evident in the crystal-orientation-induced phase shift, which can be observed not only in the thin-barrier limit but also in long junctions.

### C. Graphene-based SNS junction with $p$ -wave pairing

In recent years, extensive research works have predicted that different types of  $p$ -wave pairing symmetries can arise in graphene, either intrinsically or by the proximity effect. Uchoa *et al.* revealed that a novel singlet  $p + ip$  phase could appear in the mean-field phase diagram of graphene, featuring a gapless state with superconductivity being an underlying ordering phenomenon [67]. Subgap states in two-dimensional spectroscopy and the characteristic ABSs for the  $p_x$ - and  $p_y$ -wave pairing symmetries have been studied in

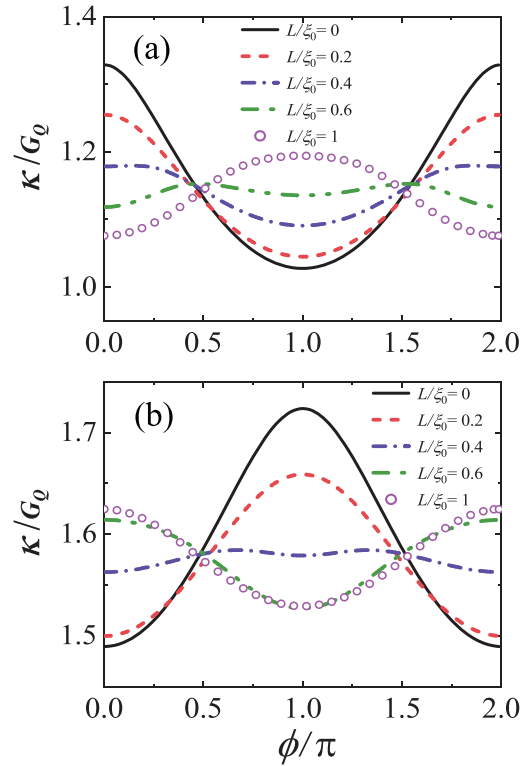


FIG. 9. Phase-dependent thermal conductance  $\kappa(\phi)$  for various junction lengths  $L/\xi_0$  at (a)  $\alpha = 0$  and (b)  $\alpha = \pi/4$ . The other parameters are the same as those in Fig. 5(a).

graphene [68]. Recently, the  $p$ -wave superconductivity was probed in single-layer graphene placed on the electron-doped cuprate superconductor  $\text{Pr}_{2-x}\text{Ce}_x\text{CuO}_4$  by using scanning tunneling spectroscopy [69]. Motivated by these experimental breakthroughs, numerous theoretical anomalous charge transport behaviors in graphene-based  $p$ -wave superconducting junctions have been reported in recent years [35,46]. In this section, we are going to determine the role of the graphene-based  $p$ -wave pairing in the heat transport. Here, we examine three different scenarios involving the junctions between two superconductors with different pairing symmetries, namely: (i)  $p_x$ - $p_x$  junction, (ii)  $p_y$ - $p_y$  junction, and (iii)  $s$ - $p_x$  junction. We assume that the quantization axis of spin (the direction of the  $\mathbf{d}$  vector) is along the  $c$  axis and parallel to the  $z$  direction, such that the spin-triplet pair potentials can be written as  $\Delta(\theta) = \Delta \cos \theta$  for  $p_x$ -wave pairing and  $\Delta(\theta) = \Delta \sin \theta$  for  $p_y$ -wave pairing [70,71].

We now study the phase dependence of thermal conductance on the  $p$ -wave pairing, as shown in Fig. 10. For the  $p_x$ - $p_x$  junction, one can see from Fig. 10(a) that the magnitude of the oscillation with respect to  $\phi$  remains nearly unchanged upon increasing  $Z$ . The situation changes, however, in the case of  $p_y$ -wave pairing, as shown in Fig. 10(b). It is observed that the oscillatory characteristics of  $\kappa(\phi)$  gradually fade out as  $Z$  increases from 0 to  $\pi/2$ . Particularly, the thermal conductance appears to be almost independent of  $\phi$  when  $Z = \pi/2$ . The physical mechanism behind this is also understood by the ABS spectrum shown in Fig. 11, where the barrier strength is fixed at  $Z = \pi/2$ .



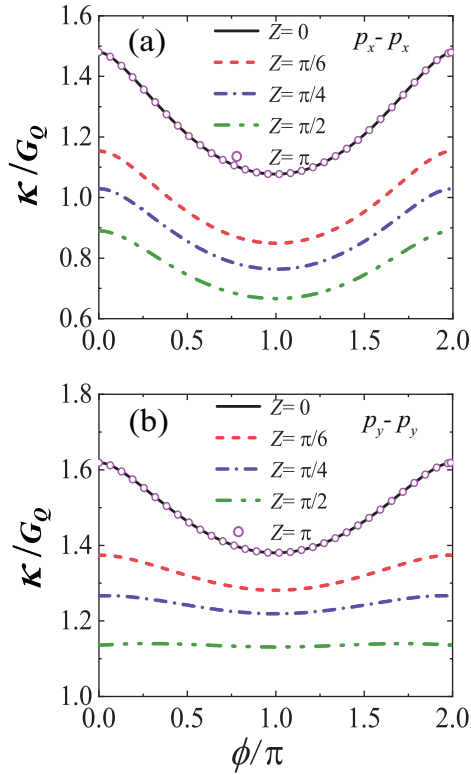


FIG. 10. Phase-dependent thermal conductance  $\kappa(\phi)$  for a series values of  $Z$  in the case of (a)  $p_x$ - $p_x$  junction and (b)  $p_y$ - $p_y$  junction. The temperature is fixed at  $T/T_c = 0.5$ .

The ABS for the  $p_x$ -wave pairing symmetry featuring ZES can be written generally as [61,71]

$$E_b(\theta, \phi) = \pm |\Delta \cos \theta| \sqrt{\sigma_n \cos(\phi/2)}. \quad (9)$$

We note that there are always a pair of ZESs located at  $\phi = \pi$  regardless of the change in  $\theta$  and  $Z$ , as shown in Fig. 11(a), which also arises from the sign change of the pair potential on the Fermi surface. These robust ZESs at  $\phi = \pi$  effectively prevent resonant tunneling, leading to the thermal conductance consistently exhibiting a minimum at  $\phi = \pi$  for any incidence and barrier strength. In contrast to the case of  $d_{xy}$  pairing, the nodal direction for  $p_x$  pairing parallels to the interface, making it difficult for quasiparticles to tunnel into the gap nodes. This explains why the amplitude of subgap transmissions is nearly negligible, as indicated in Fig. 11(a). But this is not the case for the  $p_y$ - $p_y$  junction.

The ABS for GJJs with  $p_y$ -wave pairing can be expressed as [61,71]

$$E_b(\theta, \phi) = \pm |\Delta \sin \theta| \sqrt{1 - \sigma_n \sin^2(\phi/2)}, \quad (10)$$

Since the nodal direction for  $p_y$ -wave pairing is along the interface normal, a large amount of unpaired single particles could directly tunnel into the gap nodes that are phase-independent. In addition, for small angles of incidence, the corresponding energy levels of ABSs are far from the gap edge  $\Delta$  as seen in Fig. 11(b), which in turn gives rise to a large enhancement for subgap transmissions. On the other hand, one can see that the robust ZESs are absent unlike the  $p_x$ -wave case. It follows that the effect of ABSs on the phase

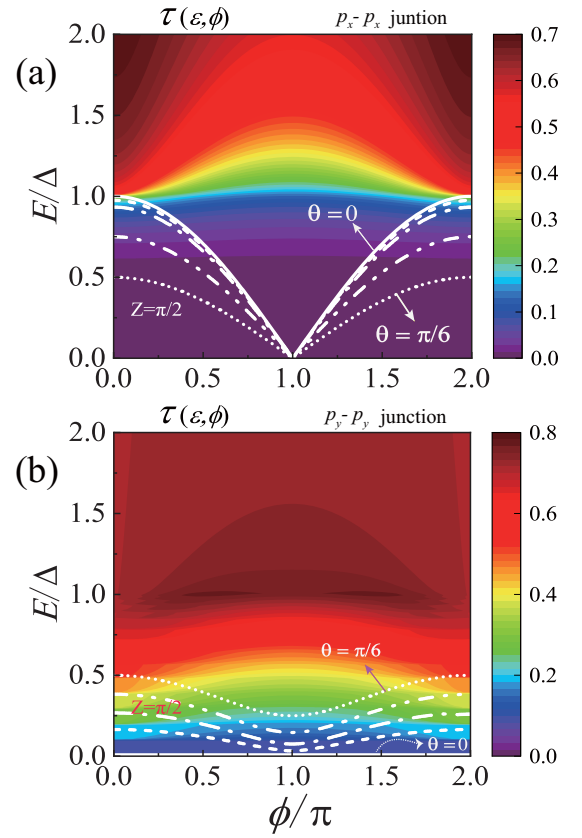


FIG. 11. Transmission function  $\tau(E, \phi)$  for (a)  $p_x$ - $p_x$  junction and (b)  $p_y$ - $p_y$  junction, corresponding to Figs. 10(a) and 10(b), respectively. White lines inside the superconducting gap indicate the energy of ABSs for various incident angles ( $\theta$ , from 0 to  $\pi/6$ ). The other parameters are the same as those in Fig. 4.

dependence of thermal conductance is diminished with the increase of  $Z$ , thereby causing the suppression of oscillatory behavior in  $\kappa(\phi)$ .

Next, we consider a junction between a singlet  $s$ -wave and a triplet  $p_x$ -wave superconductors, namely, the graphene-based  $s$ - $p_x$  junction. The junction geometry remains the same as shown in Fig. 1, with  $S_L$  representing a conventional  $s$ -wave superconductor and  $S_R$  representing a triplet  $p_x$ -wave superconductor. We choose the spin quantization axis  $z$  along the polarization vector  $\mathbf{n}$  of the triplet superconductor. As shown in Fig. 12(a), the periodicity of  $\kappa(\phi)$  changes from being  $2\pi$  periodic to being  $\pi$  periodic, with minima occurring at  $\phi = \pi/2$ . This  $\pi$  periodic behavior, as well as the amplitude of oscillation, remains robust against the interface barrier. However, it is expected that the magnitude of  $\kappa(\phi)$  will decrease when the junction transparency is reduced.

Physically, this change of periodicity can be traced back to the nontrivial spin structures of Cooper pairs. Considering the spin projection  $\sigma$  on the  $z$  axis is a good quantum number, the pairing process occurs between electrons with opposite spins in both triplet and singlet superconductors. However, the pairing potential has the same sign for  $\sigma$  and  $\bar{\sigma}$  in the triplet superconductor, while it has opposite signs in the singlet superconductor. In this case, the Cooper pairs on the left are in an  $S_z = 0$  state and have a corresponding spin structure of

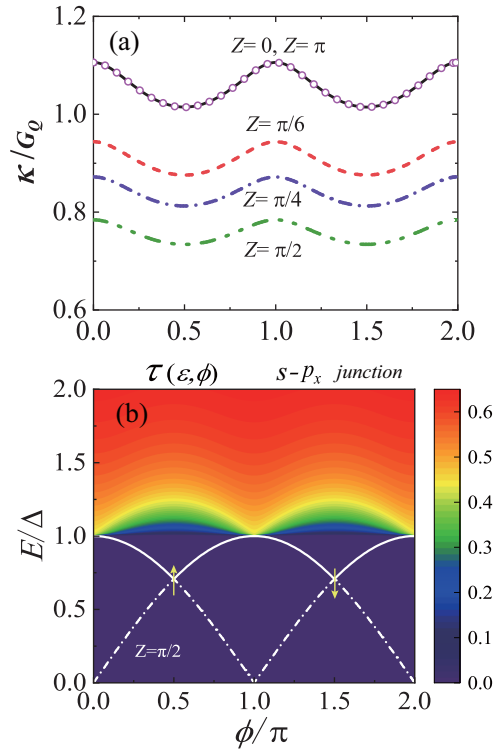


FIG. 12. (a) Phase-dependent thermal conductance  $\kappa(\phi)$  for a series values of  $Z$  for the  $s$ - $p_x$  junction. (b) The corresponding transmission function  $\tau(E, \phi)$  for  $Z = \pi/2$ . White lines inside the superconducting gap indicate the energy of ABSs at  $\theta = 0$ , where the solid and dashed lines correspond to  $E^+$  and  $E^-$ , respectively. The temperature is fixed at  $T/T_c = 0.5$ .

$\uparrow\downarrow - \downarrow\uparrow$ . On the other hand, the Cooper pairs on the right are also in an  $S_z = 0$  state but with a corresponding spin structure of  $\uparrow\downarrow + \downarrow\uparrow$ . Hence, spin conservation requires the coherent transfer of Cooper pairs, which leads to a reduced periodicity of the thermal conductance.

The change in periodicity is also reflected in the energy levels of the ABSs shown in Fig. 12(b). In this junction geometry, the phase difference across the Josephson junction is  $\phi$  for quasiparticles with  $\sigma = \uparrow$ , and  $\phi + \pi$  for  $\sigma = \downarrow$ . Hence, the energy levels of the ABSs can be determined for each  $\sigma$ :

$$E_{b\sigma}^{\pm}(\theta, \phi) = \sigma \operatorname{sgn}(\sin\phi) \Delta \sqrt{\frac{1 \pm \sqrt{1 - \sigma_n \sin^2(\phi/2)}}{2}}, \quad (11)$$

giving rise to a  $\pi$ -periodic spectrum. Furthermore, we have found that in the case of normal incidence (i.e.,  $\theta = 0$ ), the two branches of ABSs, denoted as  $E_{b\sigma}^+$  and  $E_{b\sigma}^-$ , always intersect at  $\phi = \pi/2$ . However, a gap will open between them as  $\theta$  increases, which is not shown in the figure. Actually, the phase dependence of the thermal conductance is primarily determined by  $E_{b\sigma}^+$  as it remains close to the edge of the energy gap. It is evident that the lowest energy of  $E_{b\sigma}^+$  always occurs at  $\phi = \pi/2$ . As explained earlier, this effectively prevents resonant transmission above  $\Delta$ , leading to a minimum thermal conductance at  $\phi = \pi/2$ .

Such a graphene-based  $s$ - $p_x$  junction provides a platform to explore the interplay between different superconducting

orders and offers a unique avenue for studying novel phenomena in condensed-matter physics.

#### IV. CONCLUSIONS

In this paper, we studied theoretically the phase-coherent heat transport in graphene-based SNS junctions for various types of the pairing symmetry in  $S_L$  ( $S_R$ ). The main results are as follows: (i) For  $s$ -wave pairing,  $\kappa(\phi)$  always exhibits a minimal at  $\phi = \pi$  regardless of the height of the barrier, which is in contrast with the nonrelativistic case. (ii) For  $d$ -wave pairing, by rotating the crystal orientation of  $d$ -wave superconductors,  $\kappa(\phi)$  could undergo a phase shift arising from the formation of the robust zero-energy ABSs at  $\phi = 0, 2\pi$ . This distinctive behavior cannot be qualitatively changed by the tunneling barrier or the junction length. (iii) With the increase of the tunneling barrier, the value of  $\kappa(\phi)$  for the case of  $p_y$ -pairing tends to become nearly independent of  $\phi$  due to the large number of subgap transmissions of unpaired single particles. (iv) For the  $s$ - $p_x$  junction, the periodicity of  $\kappa(\phi)$  changes from  $2\pi$  to  $\pi$ , while the minima occurs at  $\phi = \pi/2$ .

Those predicted effects are useful for detecting the phase-coherent thermal current in an actual experiment in the future. Our results are also beneficial for the application of graphene in superconducting quantum devices, particularly in the graphene-based Josephson heat interferometer. On the other hand, the phase-dependent thermal conductance contains clear signatures of the existence of ABSs, enabling experimental investigation of the pairing symmetry in graphene and opening up the possibility of exploring exotic superconductivity in two-dimensional materials through heat transport.

#### APPENDIX: SOLUTION FOR ANDREEV BOUND STATES

When considering the energy range  $E < \Delta(\theta)$  below the excitation gap, the bound states are discrete in the normal region. Such discrete Andreev levels can be written quite generally as

$$E_b(\theta, \phi) = \pm \Delta(\theta) \sqrt{1 - \sigma_n \sin^2(\phi/2)}. \quad (A1)$$

Indeed, this simplified formula obtained under the condition of  $L \ll \xi_0$  and  $E_F \gg \Delta_0$ . Specifically,  $L \ll \xi_0$  means that the length  $L$  of the normal region is small relative to the superconducting coherence length, while  $E_F \gg \Delta_0$  is required by the mean-field approximation in SCs, or equivalently, that the superconducting coherence length  $\xi = \hbar v_F / \Delta_0$  is large compared with the Fermi wavelength  $\lambda_F$  in the superconducting region.

Now we perform necessary calculation details regarding the boundary conditions and the solution for ABSs. By matching the wave functions, the boundary conditions at  $x = 0$  and  $x = L$  are respectively given by

$$\tilde{\Psi}_L|_{x=0_-} = \tilde{\Psi}_N|_{x=0_+}, \quad \tilde{\Psi}_N|_{x=L_-} = \tilde{\Psi}_R|_{x=L_+}. \quad (A2)$$

where

$$\begin{aligned} \tilde{\Psi}_L &= r_e \psi_l^{e-} + r_h \psi_l^{h+}, & \tilde{\Psi}_R &= t_e \psi_r^{e+} + t_h \psi_r^{h-}, \\ \tilde{\Psi}_N &= a \psi_n^{e+} + b \psi_n^{e-} + c \psi_n^{h+} + d \psi_n^{h-}. \end{aligned} \quad (A3)$$

Here,  $r_e$  ( $r_h$ ) and  $t_e$  ( $t_h$ ) are respectively the probability amplitudes of left- and right-moving DBdG quasiparticles in  $S_L$  and  $S_R$  regions. In the N region,  $a(b)$  and  $c(d)$  represent the probability amplitudes of right-moving (left-moving) electrons or holes. Eliminating these coefficients, one will get the homogeneous linear equations of  $f_1, f_2, f_3, \dots, f_8$ , which can be organized neatly into a matrix equation defined as  $Ay = 0$ , where the  $8 \times 8$  matrix  $A$  is a function of  $E$ ,  $\phi$ , and  $\theta$ , and  $y$  is a column vector containing eight unknown coefficients, i.e.,

$y = [r_e, r_h, a, b, c, d, t_e, t_h]^T$ . By solving this matrix equation, the ABSs can be obtained in the form of a relation between  $E$  and  $\phi$  at a given  $\theta$ , i.e., the dispersion  $E_b(\theta, \phi)$  due to the coherent subgap processes. The  $8 \times 8$  matrix  $A$  takes the form

$$A = \begin{pmatrix} A_1 & A_2 \\ A_3 & A_4 \end{pmatrix}. \quad (\text{A4})$$

Based on Eqs. (A2) and (A3), the analytical expressions for the matrices  $A_j$  can be written as follows:

$$A_1 = \begin{pmatrix} u_l^e & v_l^h & -1 & -1 \\ u_l^e e^{i\theta_e^-} & v_l^h e^{i\theta_h^+} & -e^{i\gamma_e} & e^{-i\gamma_e} \\ v_l^e e^{-i\phi_l^-} & u_l^h e^{-i\phi_l^+} & 0 & 0 \\ v_l^e e^{i\theta_e^- - i\phi_l^-} & u_l^h e^{i\theta_h^+ - i\phi_l^+} & 0 & 0 \end{pmatrix}, \quad (\text{A5})$$

$$A_2 = \begin{pmatrix} 0 & 0 & 0 & 0 \\ 0 & 0 & 0 & 0 \\ -1 & -1 & 0 & 0 \\ e^{i\gamma_h} - e^{-i\gamma_h} & 0 & 0 & 0 \end{pmatrix}, \quad (\text{A6})$$

$$A_3 = \begin{pmatrix} 0 & e^{ik_n^e L} & e^{-ik_n^e L} \\ 0 & e^{i\gamma_e + ik_n^e L} & -e^{-i\gamma_e - ik_n^e L} \\ 0 & 0 & 0 \\ 0 & 0 & 0 \end{pmatrix}, \quad (\text{A7})$$

$$A_4 = \begin{pmatrix} 0 & 0 & u_r^e e^{ik_r^e L \cos \theta_e^+} & v_r^h e^{ik_r^h L \cos \theta_h^-} \\ 0 & 0 & u_r^e e^{i\theta_e^+ + ik_r^e L \cos \theta_e^+} & v_r^h e^{i\theta_h^- + ik_r^h L \cos \theta_h^-} \\ e^{ik_n^e L} & e^{-ik_n^e L} & v_r^e e^{-i\phi_r^+ + ik_r^e L \cos \theta_e^+} & u_r^h e^{-i\phi_r^- + ik_r^h L \cos \theta_h^-} \\ -e^{i\gamma_h + ik_n^e L} & e^{-i\gamma_h - ik_n^e L} & v_r^e e^{i\theta_e^+ - i\phi_r^+ + ik_r^e L \cos \theta_e^+} & u_r^h e^{i\theta_h^- - i\phi_r^- + ik_r^h L \cos \theta_h^-} \end{pmatrix}. \quad (\text{A8})$$

Note that the definition of each element in the above matrix can be found in Sec. II. Next, we intend to elaborate on some approximate treatments used in solving the ABS.

First, the mean-field restriction that the Fermi energy  $E_F$  in the superconducting regions must be much larger than the superconducting gap, i.e.,  $E_F \gg \Delta_0$ . In our work, the Fermi energy in both  $S_L$  and  $S_R$  regions is assumed to be  $E_F = 100\Delta_0$ , which is a typical Fermi energy in doped graphene. It is necessary to point out that the linear dispersion approximation in graphene would be invalid when the Fermi energy is too large. Although  $E_F = 100\Delta_0$  is not an infinite value, this Fermi energy is large enough to satisfy the mean-field requirement, such that we can neglect the difference of the wave vectors of ELQ and HLQ in superconducting regions. In other words, we can approximate  $k_l^e = k_l^h \equiv k_S$  and  $\theta_e = \theta_h \equiv \theta_S$ .

Second, the analytical expression of the ABSs used here is only reliable in the short-junction regime, i.e.,  $L \ll \xi$ . In terms of energy scales, this condition requires  $\Delta_0 \ll \hbar v_F / L$ . In this case, the elements of  $k_n^{e(h)}(\pm E)$  and  $\gamma_{e(h)}(\pm E)$  change significantly if  $E$  is changed by at least  $\hbar v_F / L$ . Then we may thus substitute  $k_n^{e(h)}(0)$  and  $\gamma_{e(h)}(0)$  into the matrix  $A$ .

By using the two approximations mentioned above, we obtain the expression for the ABSs in terms of the normal-state transmission probability  $\sigma_n$ . This expression has the usual form for a short SNS junction, as shown in Eq. (A1). It is important to note that without these approximations, the analytical solution of ABSs would be excessively complex and not suitable for analysis.

However, the ABSs can still be evaluated numerically without any approximation. To find a nontrivial solution for the eigenvalue, it is necessary for the determinant of the matrix  $A$  to be zero, i.e.,  $(\det A) = 0$ . We have verified that the numerical results closely match the analytical solution obtained using the approximations. The simplified formulas of the ABSs are provided for the convenience of analysis in the main text, but they do not qualitatively affect our main results.

- [1] B. D. Josephson, Possible new effects in superconductive tunnelling, *Phys. Lett.* **1**, 251 (1962).
- [2] K. Maki and A. Griffin, Entropy transport between two superconductors by electron tunneling, *Phys. Rev. Lett.* **15**, 921 (1965).
- [3] K. Maki and A. Griffin, Entropy transport between two superconductors by electron tunneling, *Phys. Rev. Lett.* **16**, 258 (1966).
- [4] S. Spilla, F. Hassler, and J. Splettstoesser, Measurement and dephasing of a flux qubit due to heat currents, *New J. Phys.* **16**, 045020 (2014).
- [5] S. Spilla, F. Hassler, A. Napoli, and J. Splettstoesser, Dephasing due to quasiparticle tunneling in fluxonium qubits: A phenomenological approach, *New J. Phys.* **17**, 065012 (2015).
- [6] J. P. Pekola and B. Karimi, Colloquium: Quantum heat transport in condensed matter systems, *Rev. Mod. Phys.* **93**, 041001 (2021).
- [7] A. Fornieri and F. Giazotto, Towards phase-coherent caloritronics in superconducting circuits, *Nat. Nanotechnol.* **12**, 944 (2017).
- [8] F. Giazotto and M. J. Martínez-Pérez, The Josephson heat interferometer, *Nature (London)* **492**, 401 (2012).
- [9] M. J. Martínez-Pérez, and F. Giazotto, A quantum diffractor for thermal flux, *Nat. Commun.* **5**, 3579 (2014).
- [10] N. Ligato, F. Paolucci, E. Strambini, and F. Giazotto, Thermal superconducting quantum interference proximity transistor, *Nat. Phys.* **18**, 627 (2022).
- [11] G. Germanese, F. Paolucci, G. Marchegiani, A. Braggio, and F. Giazotto, Bipolar thermoelectric Josephson engine, *Nat. Nanotechnol.* **17**, 1084 (2022).
- [12] M. J. Martínez-Pérez and F. Giazotto, Phase-controlled superconducting heat-flux quantum modulator, *Appl. Phys. Lett.* **101**, 102601 (2012).
- [13] A. Fornieri, C. Blanc, R. Bosisio, S. D. Ambrosio, and F. Giazotto, Nanoscale phase engineering of thermal transport with a Josephson heat modulator, *Nat. Nanotechnol.* **11**, 258 (2016).
- [14] A. Fornieri, G. Timossi, P. Virtanen, P. Solinas, and F. Giazotto,  $0-\pi$  phase-controllable thermal Josephson junction, *Nat. Nanotechnol.* **12**, 425 (2017).
- [15] F. Giazotto, J. W. A. Robinson, J. S. Moodera, and F. S. Bergeret, Proximity nanovalve with large phase-tunable thermal conductance, *Appl. Phys. Lett.* **105**, 062602 (2014).
- [16] A. Fornieri, G. Timossi, R. Bosisio, P. Solinas, and F. Giazotto, Negative differential thermal conductance and heat amplification in superconducting hybrid devices, *Phys. Rev. B* **93**, 134508 (2016).
- [17] M. J. Martínez-Pérez and F. Giazotto, Efficient phase-tunable Josephson thermal rectifier, *Appl. Phys. Lett.* **102**, 182602 (2013).
- [18] F. Giazotto and F. S. Bergeret, Thermal rectification of electrons in hybrid normal metal-superconductor nanojunctions, *Appl. Phys. Lett.* **103**, 242602 (2013).
- [19] A. Fornieri, M. J. Martínez-Pérez, and F. Giazotto, A normal metal tunnel-junction heat diode, *Appl. Phys. Lett.* **104**, 183108 (2014).
- [20] M. Jo. Martínez-Pérez, A. Fornieri, and F. Giazotto, Rectification of electronic heat current by a hybrid thermal diode, *Nat. Nanotechnol.* **10**, 303 (2015).
- [21] F. Giazotto and F. S. Bergeret, Very large thermal rectification in ferromagnetic insulator-based superconducting tunnel junctions, *Appl. Phys. Lett.* **116**, 192601 (2020).
- [22] C. Guarcello, P. Solinas, A. Braggio, M. Di Ventura, and F. Giazotto, Josephson Thermal memory, *Phys. Rev. Appl.* **9**, 014021 (2018).
- [23] P. Solinas, R. Bosisio, and F. Giazotto, Microwave quantum refrigeration based on the Josephson effect, *Phys. Rev. B* **93**, 224521 (2016).
- [24] P. P. Hofer, M. Pernau-Llobet, J. B. Brask, R. Silva, M. Huber, and N. Brunner, Autonomous quantum refrigerator in a circuit QED architecture based on a Josephson junction, *Phys. Rev. B* **94**, 235420 (2016).
- [25] F. Vischi, M. Carrega, P. Virtanen, E. Strambini, A. Braggio, and F. Giazotto, Thermodynamic cycles in Josephson junctions, *Sci. Rep.* **9**, 3238 (2019).
- [26] F. S. Bergeret and F. Giazotto, Phase-dependent heat transport through magnetic Josephson tunnel junctions, *Phys. Rev. B* **88**, 014515 (2013).
- [27] B. Sothmann and E. M. Hankiewicz, Fingerprint of topological Andreev bound states in phase-dependent heat transport, *Phys. Rev. B* **94**, 081407(R) (2016).
- [28] B. Sothmann, F. Giazotto, and E. M. Hankiewicz, High-efficiency thermal switch based on topological Josephson junctions, *New J. Phys.* **19**, 023056 (2017).
- [29] A. Mukhopadhyay and S. Das, Thermal signature of the Majorana fermion in a Josephson junction, *Phys. Rev. B* **103**, 144502 (2021).
- [30] A. G. Bauer, B. Scharf, L. W. Molenkamp, E. M. Hankiewicz, and B. Sothmann, Quantized phase-coherent heat transport of counterpropagating Majorana modes, *Phys. Rev. B* **104**, L201410 (2021).
- [31] A. G. Bauer and B. Sothmann, Phase-dependent heat transport in Josephson junctions with  $p$ -wave superconductors and superfluids, *Phys. Rev. B* **99**, 214508 (2019).
- [32] S. Y. Hwang and B. Sothmann, Phase-coherent caloritronics with ordinary and topological Josephson junctions, *Eur. Phys. J. Spec. Top.* **229**, 683 (2020).
- [33] T. Savander, S. Tamura, C. Flindt, Y. Tanaka, and P. Buset, Thermoelectric detection of Andreev states in unconventional superconductors, *Phys. Rev. Res.* **2**, 043388 (2020).
- [34] D. Perconte, D. Bercioux, B. Dlubak, P. Seneor, F. S. Bergeret, and J. E. Villegas, Superconducting proximity effect in  $d$ -wave cuprate/graphene heterostructures, *Ann. Phys. (Berlin, Ger.)* **534**, 2100559 (2022).
- [35] C. S. Huang and Y. C. Tao, Identifying the graphene  $p$ -wave superconducting symmetry by conductance and shot noise oscillations, *Phys. Lett. A* **384**, 126502 (2020).
- [36] G. H. Lee and H.-J. Lee, Proximity coupling in superconductor-graphene heterostructures, *Rep. Prog. Phys.* **81**, 056502 (2018).
- [37] C. S. Huang, Y. J. Wei, Y. C. Tao, and J. Wang, Spin-orbit coupling assisted magnetoanisotropic Josephson effect in ferromagnetic graphene Josephson junctions, *Phys. Rev. B* **103**, 035418 (2021).
- [38] C. W. J. Beenakker, Colloquium: Andreev reflection and Klein tunneling in graphene, *Rev. Mod. Phys.* **80**, 1337 (2008).
- [39] L. Brey and H. A. Fertig, Electronic states of graphene nanoribbons studied with the Dirac equation, *Phys. Rev. B* **73**, 235411 (2006).

- [40] C. W. J. Beenakker, Specular Andreev reflection in graphene, *Phys. Rev. Lett.* **97**, 067007 (2006).
- [41] A. H. Castro Neto, F. Guinea, N. M. R. Peres, K. S. Novoselov, and A. K. Geim, The electronic properties of graphene, *Rev. Mod. Phys.* **81**, 109 (2009).
- [42] J. Ren and J.-X. Zhu, Anomalous energy transport across topological insulator superconductor junctions, *Phys. Rev. B* **87**, 165121 (2013).
- [43] M. Titov and C. W. J. Beenakker, Josephson effect in ballistic graphene, *Phys. Rev. B* **74**, 041401(R) (2006).
- [44] P. N. Butcher, Thermal and electrical transport formalism for electronic microstructures with many terminals, *J. Phys.: Condens. Matter* **2**, 4869 (1990).
- [45] C. L. Kane and M. P. A. Fisher, Quantized thermal transport in the fractional quantum Hall effect, *Phys. Rev. B* **55**, 15832 (1997).
- [46] C. S. Huang, Y. Yang, and Y. C. Tao, Anomalous zero bias conductance peaks in a graphene-based ferromagnet/insulator/ $p$ -wave superconductor hybrid structure, *Superlattices Microstruct.* **133**, 106201 (2019).
- [47] C. S. Huang, Y. Yang, Y. C. Tao, and J. Wang, Identifying the graphene  $d$ -wave superconducting symmetry by an anomalous splitting zero-bias conductance peak, *New J. Phys.* **22**, 033018 (2020).
- [48] C. S. Huang and Y. C. Tao, Anomalous zero bias conductance peak in a ferromagnetic graphene junction with  $d$ -wave anisotropic superconducting pair symmetry, *AIP Adv.* **9**, 075319 (2019).
- [49] R. Franz and G. Wiedemann, Ueber die Wärme-Leitungsfähigkeit der Metalle, *Ann. Phys. (Berlin, Ger.)* **165**, 497 (1853).
- [50] C. W. J. Beenakker, Universal limit of critical-current fluctuations in mesoscopic Josephson junctions, *Phys. Rev. Lett.* **67**, 3836 (1991).
- [51] M. Maiti and K. Sengupta, Josephson effect in graphene superconductor/barrier/superconductor junctions: Oscillatory behavior of the Josephson current, *Phys. Rev. B* **76**, 054513 (2007).
- [52] G. Nanda, J. L. Aguilera-Servin, P. Rakyta, A. Kormányos, R. Kleiner, D. Koelle, K. Watanabe, T. Taniguchi, L. M. K. Vandersypen, and S. Goswami, Current-phase relation of ballistic graphene Josephson junctions, *Nano Lett.* **17**, 3396 (2017).
- [53] D. A. Manjarrés, S. Gómez Páez, and W. J. Herrera, Skewness and critical current behavior in a graphene Josephson junction, *Phys. Rev. B* **101**, 064503 (2020).
- [54] D. I. Indolese, P. Karnatak, A. Kononov, R. Delagrangé, R. Haller, L. Wang, P. Makk, K. Watanabe, T. Taniguchi, and C. Schönenberger, Compact SQUID realized in a double-layer graphene heterostructure, *Nano Lett.* **20**, 7129 (2020).
- [55] R. Haller, G. Fülöp, D. Indolese, J. Ridderbos, R. Kraft, L. Y. Cheung, J. H. Ungerer, K. Watanabe, T. Taniguchi, D. Beckmann, R. Danneau, P. Virtanen, and C. Schönenberger, Thermoelectric detection of Andreev states in unconventional superconductors, *Phys. Rev. Res.* **4**, 013198 (2022).
- [56] A. M. Black-Schaffer and C. Honerkamp, Chiral  $d$ -wave superconductivity in doped graphene, *J. Phys.: Condens. Matter* **26**, 423201 (2014).
- [57] Y. Q. Li and T. Zhou, Impurity effect as a probe for the pairing symmetry of graphene-based superconductors, *Front. Phys.* **16**, 43502 (2021).
- [58] D. Perconte, K. Seurre, V. Humbert, C. Ulysse, A. Sander, J. Trastoy, V. Zlatko, F. Godel, P. R. Kidambi, S. Hofmann, X. P. Zhang, D. Bercioux, F. S. Bergeret, B. Dlubak, P. Seneor, and Javier E. Villegas, Long-range propagation and interference of  $d$ -wave superconducting pairs in graphene, *Phys. Rev. Lett.* **125**, 087002 (2020).
- [59] F. A. Cuellar, C. Moreau-Luchaire, M. Piquemal-Banci, R. Galceran, P. R. Kidambi, M. B. Martin, S. Hofmann, R. Bernard, B. Dlubak, P. Seneor, and J. E. Villegas, Tunable Klein-like tunnelling of high-temperature superconducting pairs into graphene, *Nat. Phys.* **14**, 25 (2018).
- [60] Q. J. Sun, H. S. Wang, H. M. Wang, L. W. Deng, Z. W. Hu, B. Gao, Q. Li, and X. M. Xie, Electronic transport transition at graphene/YBa<sub>2</sub>Cu<sub>3</sub>O<sub>7</sub> junction, *Appl. Phys. Lett.* **104**, 102602 (2014).
- [61] J. Linder, A. M. Black-Schaffer, T. Yokoyama, S. Doniach, and A. Sudbø, Josephson current in graphene: Role of unconventional pairing symmetries, *Phys. Rev. B* **80**, 094522 (2009).
- [62] H. Goudarzi, M. Khezerlou, and H. Kamalipour, Strained graphene Josephson junction with anisotropic  $d$ -wave superconductivity, *Superlattices Microstruct.* **83**, 101 (2015).
- [63] S. Kashiwaya and Y. Tanaka, Tunnelling effects on surface bound states in unconventional superconductors, *Rep. Prog. Phys.* **63**, 1641 (2000).
- [64] Y. S. Barash, H. Burkhardt, and D. Rainer, Low-temperature anomaly in the Josephson critical current of junctions in  $d$ -wave superconductors, *Phys. Rev. Lett.* **77**, 4070 (1996).
- [65] C.-R. Hu, Midgap surface states as a novel signature for  $d_{x^2-y^2}$ -wave superconductivity, *Phys. Rev. Lett.* **72**, 1526 (1994).
- [66] Y. Tanaka and S. Kashiwaya, Theory of tunneling spectroscopy of  $d$ -wave superconductors, *Phys. Rev. Lett.* **74**, 3451 (1995).
- [67] B. Uchoa and A. H. Castro Neto, *Phys. Rev. Lett.* **98**, 146801 (2007).
- [68] O. E. Casas, S. G. Paez, A. L. Yeyati, P. Bursset, and W. J. Herrera, Subgap states in two-dimensional spectroscopy of graphene-based superconducting hybrid junctions, *Phys. Rev. B* **99**, 144502 (2019).
- [69] A. Di Bernardo, O. Millo, M. Barbone, H. Alpern, Y. Kalcheim, U. Sassi, A. K. Ott, D. De Fazio, D. Yoon, M. Amado1, A. C. Ferrari, J. Linder, and J. W. A. Robinson,  $p$ -wave triggered superconductivity in single-layer graphene on an electron-doped oxide superconductor, *Nat. Commun.* **8**, 14024 (2017).
- [70] T. Hirai, Y. Tanaka, N. Yoshida, Y. Asano, J. Inoue, and S. Kashiwaya, Temperature dependence of spin-polarized transport in ferromagnet/unconventional superconductor junctions, *Phys. Rev. B* **67**, 174501 (2003).
- [71] X. Li, Josephson current in  $p$  wave pairing superconductor graphene junctions, *Solid State Commun.* **151**, 1976 (2011).